

A quantum trampoline for ultra-cold atoms

M. ROBERT-DE-SAINT-VINCENT¹, J.-P. BRANTUT¹, CH.J. BORDÉ², A. ASPECT¹, T. BOURDEL¹ and P. BOUYER¹

¹ *Laboratoire Charles Fabry de l'Institut d'Optique, Univ Paris Sud, CNRS, campus polytechnique RD128, 91127 Palaiseau, France*

² *SYRTE, Observatoire de Paris, CNRS, UPMC, 61 avenue de l'Observatoire, 75014 Paris, France*

PACS 03.75.Dg – Atom and neutron interferometry
 PACS 06.30.Gv – Velocity, acceleration, and rotation
 PACS 05.60.Gg – Quantum transport

Abstract. – We have observed the interferometric suspension of a free-falling Bose-Einstein condensate periodically submitted to multiple-order diffraction by a vertical 1D standing wave. The various diffracted matter waves recombine coherently, resulting in high contrast interference in the number of atoms detected at constant height. For long suspension times, multiple-wave interference is revealed through a sharpening of the fringes. We use this scheme to measure the acceleration of gravity.

Introduction. – Atoms in free fall are remarkable test masses for measuring gravity, with a host of applications from underground survey to tests of the equivalence principle [1]. Because of the quantized character of atom-light interaction, the acceleration of free falling atoms can be precisely measured with lasers, for instance by comparing the velocity change of atoms by absorption or emission of a single photon to the gravity induced velocity change in a precisely determined time [2]. Furthermore, atom interferometry exploits the quantum nature of matter-waves [3–6]. In both cases, an accurate measurement of gravity demands a long time of free fall, but it is a priori limited by the size of the vacuum chamber in which the measurement takes place [7–9]. It is possible to overcome this limitation by bouncing many times the atoms on an atomic mirror [10], realizing a trampoline for atoms [11,12]. This scheme can be used to fold the trajectories within a standard light-pulse atom gravimeter [12].

Here we show how to operate a quantum trampoline based on a periodically applied imperfect Bragg mirror, which not only reflects upwards the falling atoms, but also acts as a beam splitter that separates and recombines the atomic wave packets. This results in multiple-wave [13–16] atom interference, evidenced by an efficient suspension of the atoms even though successive leaks at each imperfect reflection would classically lead to a complete loss of the atoms. This suspension is obtained at a precise tuning of the trampoline period, whose value yields directly the local value of gravity g . Our scheme can be generalized to

other interferometer geometries, such as in [17,18] replacing perfect Bragg reflections with imperfect ones.

A classical trampoline for atoms can be experimentally realized by periodically bouncing them with perfect Bragg mirrors. These mirrors are based on atom diffraction by a periodic optical potential [19], i.e. a vertical standing wave of period $\lambda/2$, where λ is the laser wavelength. The interaction between the atoms and the optical potential leads to vertical velocity changes quantized in units of $2V_R$, where $V_R = h/\lambda m$ is the one photon recoil velocity of an atom of mass m (h is the Planck constant). For long interaction pulses, the applied potential can be considered as time independent, and the atom kinetic energy has to be conserved. This requirement is fulfilled by changing the vertical velocity component from $-V_R$ to $+V_R$, and vice-versa. We call this process a resonant velocity transfer. Perfect Bragg reflection, yielding only resonant velocity transfer, is obtained by choosing appropriate duration and intensity of the pulse [12]. When a perfect Bragg reflection is applied on atoms freely falling with a velocity $-V_R$, they bounce upward with a velocity $+V_R$. After a time $T_0 = 2V_R/g$ (≈ 1.2 ms for ^{87}Rb), the reflected atoms have again a velocity $-V_R$ because of the downwards acceleration of gravity g . Repeating this sequence with a period T_0 allows to suspend the atoms at an almost constant altitude (thick line in Fig. 1). This is a classical trampoline [11,12].

To operate the trampoline in the quantum regime, we use imperfect Bragg reflections, associated with short laser

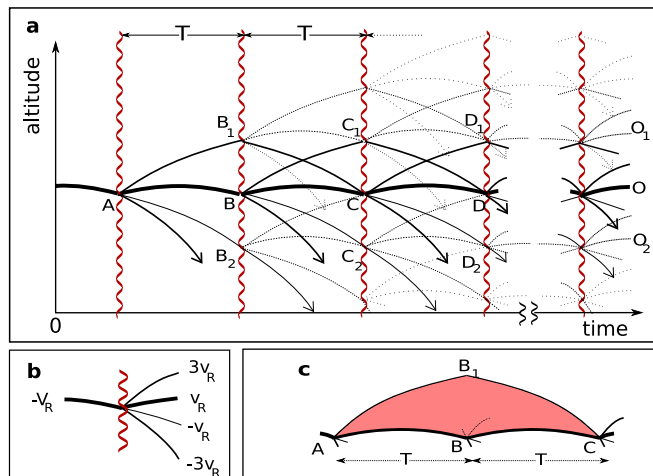


Fig. 1: Atom trajectories in the quantum trampoline. **a**, atoms, diffracted by periodically applied imperfect Bragg mirror, explore various paths which eventually recombine. The probability of a trajectory is represented by the line thickness. The thick line corresponds to a classical trampoline associated with perfect Bragg reflections. The arrows mark the loss channels at $-3V_R$. **b**, an imperfect Bragg reflection: an incoming matter-wave with vertical velocity $-V_R$ is mainly Bragg reflected to $+V_R$ (thick line). A small fraction is also diffracted to higher velocities ($+3V_R$ and $-3V_R$), and a smaller one transmitted without deviation. **c**, elementary interferometer: from a zero-order trajectory (thick line), an atom can be diffracted to $+3V_R$, at point A in the example shown. It is then Bragg reflected from $+V_R$ to $-V_R$ at point B₁ one period later, and finally recombines at point C with the zero-order trajectory, thanks to diffraction from $-3V_R$ to $+V_R$.

pulses, for which the kinetic energy conservation requirement is relaxed: Heisenberg time-energy relation permits energy to change by about h/τ for a pulse of duration τ . Choosing $\tau \approx h/4mV_R^2$ allows us to obtain additional velocity changes from $-V_R$ to secondary diffracted components with velocities $\pm 3V_R$ (Fig. 1b), hereafter referred as non-resonant velocity transfers. The matter-wave packet is thus split into various components that eventually recombine, resulting in a richer situation where atomic interference plays a dramatic role (Fig. 1a). For our experimental conditions ($\tau \approx 35 \mu\text{s}$), transition from $-V_R$ to $+V_R$ occurs with a probability of 0.93, while the amplitudes ϵ of the components diffracted to $\pm 3V_R$ correspond to a probability $|\epsilon|^2 \approx 0.03$ ($|\epsilon| \approx 0.17$). The amplitudes of higher velocity components are negligible, and the probability to remain at $-V_R$ is 0.01. A similar situation occurs for an atom with initial velocity $+V_R$: transition to $-V_R$ happens with probability 0.93 and to $\pm 3V_R$ with probability $|\epsilon|^2 \approx 0.03$.

We operate our quantum trampoline as follows. An all-optically produced ultra-cold sample of 1.5×10^5 ^{87}Rb atoms in the $F = 1$ hyperfine level [20] is released from the trap with a rms vertical velocity spread of $0.1 V_R$ for the Bose-Einstein condensate and $0.6 V_R$ for the thermal

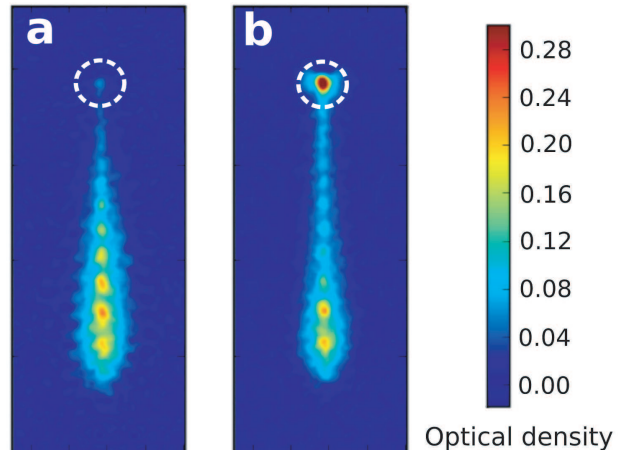


Fig. 2: Outputs and losses in a 15-pulse quantum trampoline. **a** and **b**, absorption images taken 2 ms after the last pulse (O in Fig. 1), in the case of destructive (**a**) and constructive (**b**) interference in the suspended channel. The pulse periods are $T=1.206$ ms and $T=1.198$ ms respectively. The image extends over 3 mm vertically. The atoms suspended against gravity lie in the circle at the top of the images. The spots below correspond to loss channels and are strongly suppressed in **b** compared to **a** due to the interference blocking the loss channels. The two lowest spots correspond to losses at points A and B of Fig. 1a, which cannot be suppressed by interference.

cloud. In this work, the condensate fraction is limited to 0.2. After $600 \mu\text{s}$ ($\approx T_0/2$) of free fall, such that the mean atomic velocity reaches $-V_R$ because of gravity, we start to apply imperfect Bragg reflections with a period T , close to the classical suspension period T_0 . More precisely, a retroreflected circularly-polarized beam of intensity 4 mW, 6.3 GHz red-detuned with respect to the nearest available atomic transition from $F = 1$ is then periodically applied for a pulse duration $\tau \approx 35 \mu\text{s}$. The successive diffraction events result in several atomic trajectories that coherently recombine in each output channel, as presented in Fig. 1a.

After N pulses, we wait for a 2 ms time of flight and detect the atoms through absorption imaging with resonant light. We observe distinct wave-packets (Fig. 2). The atoms situated in the circle at the top have been suspended against gravity, while the distinct packets below correspond to falling atoms. These atoms have acquired a velocity $-3V_R$ after one of the laser pulses, and then continue to fall, unaffected by the subsequent pulses. The difference between Fig. 2a and 2b shows that a small change in the pulse period T results in a dramatic change in the number of suspended atoms. When suspension is maximum (Fig. 2b), the losses are strongly suppressed except for the two lowest spots, which correspond to atoms that have been lost at points A and B of Fig. 1. This behavior is due to quantum interferences between the vari-

ous trajectories as presented in Fig. 1a : for an adequate pulse period T , the interferences are constructive in the suspended trajectories and destructive in the falling ones, except at points A and B where no interference can happen. This blocking of the 'leaking channels' is analogous to the suppression of light transmission through a multi-layer dielectric mirror.

Our quantum trampoline is a multiple-wave interferometer, where the fraction of atoms in each output port is equal to the square modulus of the sum of the amplitudes associated with all trajectories that coherently recombine at the end. We classify the contributing trajectories with respect to the number of non-resonant velocity transfers. The zero-order path is the one which is reflected from $-V_R$ to $+V_R$ at each pulse (trajectory ABCD...O in Fig. 1a and Fig. 1c). This is the path associated with the largest output amplitude (of square modulus 0.93^N). The first-order paths are the ones which are once deviated upwards from the zero-order path, and recombine with it after twice the period T (for example, the trajectories $AB_1CD...O$ or $ABC_1D...O$ in Fig. 1a). All these paths have the same accumulated interferometric phase that depends on the pulse period T . Their amplitude, proportional to $|\epsilon|^2$, is small but the number of such paths increases as the number of pulses N . Their total contribution to the probability amplitude at O scales as $N|\epsilon|^2$. Higher order paths, with more than 2 non-resonant transfers, are less probable individually, but their number increases faster with the number of pulses. As a consequence, they can have a major contribution to the final probability amplitude. More precisely, multiple-wave interference plays an important role when $N|\epsilon|^2$ becomes of the order of 1.

Figure 3 shows the fraction of suspended atoms for a 10-pulse quantum trampoline where the interference between the zero- and first-order paths dominates since $N|\epsilon|^2 \approx 0.3$ is small compared to 1. When the pulse period T is changed, we observe interference fringes with characteristic spacing $\Delta T = 16.6(2) \mu s$, in agreement with the calculation for the elementary interferometer (Fig. 1c) [21]: $\Delta T = \lambda/4gT$. We also observe an additional modulation with a fringe spacing of $\Delta T' = 33 \mu s$, about twice ΔT . It can be understood by considering the interferometers from A to O_1 and from A to O_2 , such as $AB_1C_1D_1...O_1$ and $ABC_1D_1...O_1$. The corresponding fringe spacing $\Delta T' = \lambda/4|V_R - gT|$ is equal to $2\Delta T$ for $T = T_0$. The output ports O_1, O_2 of these additional interferometers are $14 \mu m$ above or below O. In our absorption images, we do not distinguish the various ports and the observed signal is thus the sum of the intensities of the two fringe patterns. In addition, the total interference pattern is included in a broad envelop due to the mirror velocity selectivity as predicted for a classical trampoline in [11] and first observed in [12].

We model our quantum trampoline in a semi-classical approximation [22]. It makes use of complex amplitudes calculated along the classical trajectories plotted in Fig. 1a. During each free-fall, the accumulated phase is given by the action along the trajectory and, for each

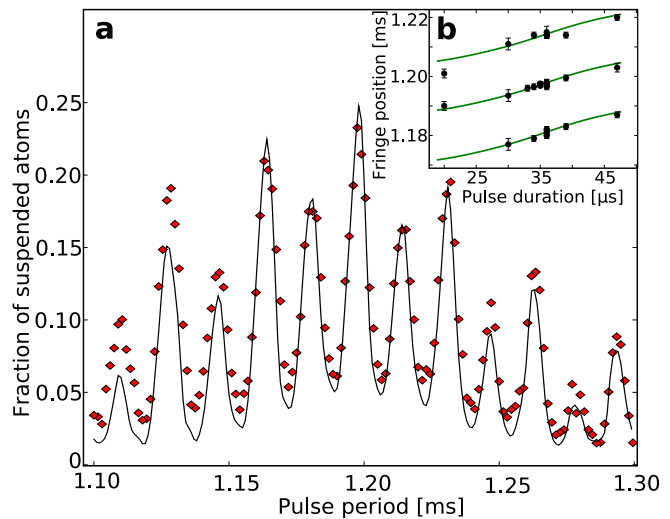


Fig. 3: Interference fringes for a 10-pulse quantum trampoline. **a**, fraction of suspended atom as a function of the pulse period. The overall envelope is due to the velocity selectivity [11] while the modulation is due to quantum interference. The solid line corresponds to our model as presented in the text. **b**, position of three consecutive fringe maxima around the highest maximum, as a function of the pulse duration, showing the influence of the phase shift ϕ_0 imprinted by the diffraction pulses : Dots are experimental points, with error bars reflecting the experimental uncertainties. Solid lines come from the theoretical model using $g=9.809 \text{ m.s}^{-2}$.

diffraction pulse, the matrix of transfer amplitudes between the various inputs and outputs is calculated by solving the Schrödinger equation in momentum space. At each output O of the interferometer, we sum the amplitudes of all possible trajectories from the input A to that output and take the square modulus to get its probability. For comparison with our observations, the fraction of suspended atoms is taken as the sum of the probabilities at all outputs O_i . Finally, we take into account the finite temperature of the initial atomic sample by summing the results over the distribution of initial velocities. This model reproduces accurately the whole interference pattern of Fig. 3a.

When we increase the number of pulses so that $N|\epsilon|^2 \approx 1$, the contribution from higher order paths is not negligible and we enter a regime of multiple-wave interference. Fig. 4a shows a comparison of the fringes for the cases of 10 and 20 consecutive pulses. After 20 pulses, we observe a clear deviation from a sinusoidal pattern, the fringe width decreases and the contrast increases to almost 1. As plotted in Fig. 4b, the fringe half-width at half-maximum decreases from $4.1 \mu s$ after 10 pulses, where $N|\epsilon|^2 \approx 0.3$, to $2.1 \mu s$ after 30 pulses, where $N|\epsilon|^2 \approx 0.3$. The relative contributions to the output amplitude at O of zero-, first-, and second-order paths increase from 1, 0.26, and 0.01 respectively in the case of 10 pulses to 1, 0.9, 0.32 in the case of 30 pulses. The finesse of our interferometer, i.e. the ratio of the full-width at half-maximum of the resonances to

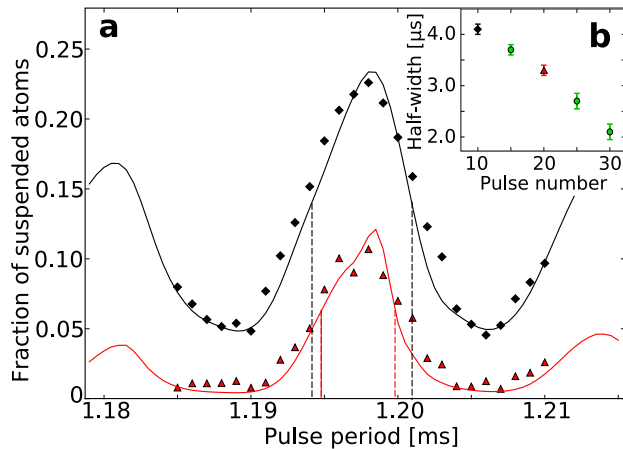


Fig. 4: Multiple-wave quantum trampoline. **a**, suspended fraction as a function of the pulse period, for 10 (diamonds) and 20 (triangles) pulses. The contrast evolves from 0.6 to almost 1 and the fringe width is significantly reduced as highlighted by the vertical dashed lines at half-maximum. Lines : calculated suspended fraction, with $g = 9.809 \text{ m.s}^{-2}$ selected as fitting parameter. **b**, fringe half-width at half-maximum as a function of the number of pulses N . The narrowing of the fringes with increasing N is an evidence of the stronger contribution of higher order paths to the interference pattern.

the fringe spacing, is 4 after 30 pulses. This increase of the finesse is an evidence of the stronger contribution of the higher order paths when the number N of pulses increases, as expected for a multiple-wave interferometer [13–15].

Our quantum trampoline is sensitive to gravity. From the position of the broad envelop associated with the classical trampoline, we can deduce $g=9.8(1)$. The same value, with a similar accuracy can also be inferred from the fringe spacing. However, a measure of the absolute fringe position allows us to reach a better accuracy. For this, we need to take into account an additional phase [21] ϕ_0 resulting from the diffraction events, which varies with the pulse duration (Fig. 3b). We calculate precisely this phase with our model, and use it to fit the data on Fig. 4a with g as the only fitting parameter. We find $g = 9.809(4) \text{ m.s}^{-2}$, in agreement with the known value of g in Palaiseau (9.8095 m.s^{-2} from WGS84). The uncertainty is due to our signal-to-noise ratio, and to standing-wave power fluctuations which affect the complex diffraction amplitudes. There are several possibilities to improve our setup. First, a higher number of bounces is achievable, for example starting from a condensate in a trap with weaker confinement, for which the velocity spread after release is reduced [12]. Second, an adequate shaping of the pulses temporal envelope [23] could favor well chosen diffracted orders, and increase the number of contributing trajectories, resulting into a higher finesse of the fringe pattern. Third, using a standing wave with a smaller wavelength or atoms with a reduced mass (such as helium or lithium),

the time between bounces would increase and the precision on g could be improved by several orders of magnitudes.

Conclusion. – We have presented a quantum trampoline and used it as a proof-of-principle simple and compact gravimeter, where atoms are held in a volume of few cubic micrometers. Further investigations are needed to study the systematic effects and limitations of our interferometric scheme and to compare it with other compact sensors [2, 12, 27]. Our scheme, where the atomic wavefunction is repeatedly split and recombined, is likely to be weakly sensitive to atom interaction or to laser phase-noise thanks to averaging over many diffraction events. Beyond the prospect of miniaturized gravito-inertial sensors, our setup has potential applications for measuring fundamental forces at small distances [25, 26]. It also opens perspectives for new types of interferometers and new sensor geometries. Suspended atoms could be used for atomic clock applications [16] or to build additional interferometers in the horizontal plane. The interrogation time would then not be limited by the size of the experimental chamber. The realization of a multidimensional interferometer measuring simultaneously the acceleration in three dimensions seems possible [24]. Our quantum trampoline differs dramatically from its classical analogue, where the random velocity transfers would result in atom losses. It provides another clear demonstration of the dichotomy between classical and quantum dynamics [28–30].

We acknowledge F. Moron and A. Villing for technical assistance, R. A. Nyman, J.-F. Clément and B. Allard for their work on the apparatus, F. Impens for helpful discussions. This research was supported by CNRS, CNES as part of the ICE project, Direction Générale de l’Armement, the project “blanc” MélaBoFérIA from ANR, IFRAF ; by the STREP program FINAQS of the European Union and by the MAP program SAI of the European Space Agency (ESA).

REFERENCES

- [1] FRAY S., DIEZ C.A., HÄNSCH T.W. and WEITZ M., *Phys. Rev. Lett.*, **93** (240404) 2004.
- [2] CLADÉ P. *et al.*, *Europhys. Lett.*, **71** (730) 2005.
- [3] CRONIN A.D., SCHMIEDMAYER J. and PRITCHARD, D.E., *Rev. Mod. Phys.*, **81** (1051) 2009.
- [4] BERMAN P.R. (Editor), *Atom Interferometry* (Academic Press, City) 1997.
- [5] PETERS A., CHUNG K.Y. and CHU S., *Metrologia*, **38** (25) 2001.
- [6] SNADDEN M.J., MCGUIRK J.M., BOUYER P., HARITOS K.G. and KASEVICH M.A., *Phys. Rev. Lett.*, **81** (971) 1998.
- [7] DIMOPOULOS S., GRAHAM P.W., HOGAN J.M. and KASEVICH M.A., *Phys. Rev. D*, **78** (042003) 2008.
- [8] VOGEL A. *et al.*, *Appl. Phys. B*, **84** (663) 2006.
- [9] STERN G. *et al.*, *Euro. Phys. Jour. D*, **53** (353) 2009.

- [10] AMINOFF C.G. *et al.*, *Phys. Rev. Lett.*, **71** (3083) 1993.
- [11] IMPENS F., BOUYER P. and BORDÉ C.J., *Appl. Phys. B*, **84** (603) 2006.
- [12] HUGHES K.J., BURKE J.H.T. and SACKETT C.A., *Phys. Rev. Lett.*, **102** (150403) 2009.
- [13] WEITZ M., HEUPEL T. and HÄNSCH T.W., *Phys. Rev. Lett.*, **77** (2356) 1996.
- [14] HINDERTHÜR H. *et al.*, *Phys. Rev. A*, **59** (2216) 1999.
- [15] AOKI T., SHINOHARA K. and MORINAGA A., *Phys. Rev. A*, **63** (063611) 2001.
- [16] IMPENS F. and BORDÉ, C.J., *Phys. Rev. A*, **80** (031602) 2009.
- [17] RASEL E.M., OBERTHALER M.K., BATELAAN H., SCHMIEDMAYER J. and ZEILINGER A., *Phys. Rev. Lett.*, **75** (2633) 1995.
- [18] GUPTA S., DIECKMANN K., HADZIBABIC Z. and PRITCHARD D.E., *Phys. Rev. Lett.*, **89** (140401) 2002.
- [19] KOZUMA M. *et al.*, *Phys. Rev. Lett.*, **82** (871) 1999.
- [20] CLÉMENT J.-F. *et al.*, *Phys. Rev. A*, **79** (061406(R)) 2009.
- [21] The calculation of the phase difference for the elementary interferometer (Fig. 1c) leads to $\Delta\phi = \phi_0 - 4\pi gT^2/\lambda$, where ϕ_0 is a constant resulting from the sum of the phase shifts acquired during the diffraction events. The trajectory AB₁C...O experiences two non-resonant transfers while ABC...O experiences none.
- [22] Our semi-classical approximation can be justified by decomposing the sample into a superposition of Heisenberg limited wave-packets with a momentum spread Δp and position spread Δx such that (i) $(\Delta p/m)NT < \Delta x$, (ii) $\Delta p/m \ll V_R$, and (iii) $\Delta x < 14 \mu\text{m}$ (NT is the total duration of the interferometer). In our case, these conditions are met for $\Delta x \approx 10 \mu\text{m}$. During the free falls, according to condition (i), the expansion of a wave-packet can be neglected and the exact ABCD formalism [32,33] reduces to calculating its classical trajectory (position and momentum) and the classical action along it. For the pulses, condition (ii) ensures that the momentum spread is sufficiently low so that the diffraction amplitudes can be calculated as for plane waves. Finally, condition (iii) implies that wave-packets ending at different positions do not overlap. For the condensate part, the previous description is also valid as the interactions ensure that the initial spatial coherence is lost because the chemical potential $\mu \approx 1 \text{ kHz}$ is such that $\mu NT/h \gg 1$.
- [23] KELLER C. *et al.*, *Appl. Phys. B*, **69** (303) 1999.
- [24] BORDÉ C.J., *Gen. Relativ. Gravit.*, **36** (475) 2004.
- [25] CARUSOTTO I., PITAEVSKII L., STRINGARI S., MODUGNO G. and INGUSCIO M., *Phys. Rev. Lett.*, **95** (093202) 2005.
- [26] HARBER D.M., OBRECHT J.M., MCGUIRK J.M. and CORNELL E.A., *Phys. Rev. A*, **72** (033610) 2005.
- [27] FERRARI G., POLI N., SORRENTINO F. and TINO G.M., *Phys. Rev. Lett.*, **97** (060402) 2006.
- [28] MOORE F.L., ROBINSON J.C., BHARUCHA C., WILLIAMS P.E. and RAIZEN M. G., *Phys. Rev. Lett.*, **73** (2974) 1994.
- [29] RYU C. *et al.*, *Phys. Rev. Lett.*, **96** (160403) 2006.
- [30] KEMPE J., *Contemporary Physics*, **50** (339) 2009.
- [31] KINOSHITA T., WENGER T. and WEISS D.S., *Phys. Rev. A*, **71** (011602) 2005.
- [32] BORDÉ C.J., *C. R Acad. Sc. - series IV - Physics*, **2** (509) 2001.
- [33] BORDÉ C.J., *Metrologia*, **39** (435) 2002.